Do Dissolving Objects Converge to a Universal Shape?

Elias Nakouzi[†], Raymond E. Goldstein[‡], and Oliver Steinbock[†*]

[†] Department of Chemistry and Biochemistry, Florida State University, Tallahassee, FL 32306-4390, USA

[‡] DAMTP, Centre for Mathematical Sciences, University of Cambridge, Cambridge CB3 0WA, UK

Surprisingly, macroscopic objects such as melting ice cubes and growing stalactites approach non-intuitive geometric ideals. Here we investigate the shape of dissolving cylinders in a large volume of water. The cylinders are oriented vertically and consist of amorphous glucose or polyethylene glycol. The dissolution causes density differences in the surrounding fluid, which induce gravity-driven convection downwards along the object. The resulting concentration gradient shapes the cylinder according to fast dissolution at the tip and slow dissolution at the base. The contour of the object approaches a power law of the form $z \propto R^2$ where z is the vertical distance from the tip and R is the corresponding radius. We suggest that this paraboloidal shape is the geometric attractor for the dissolution of non-crystalline objects in the presence of gravity.

Keywords: Dissolution, convection, paraboloid, tip, free-boundary problem, power law

INTRODUCTION

Nature creates a wealth of macroscopic objects that are shaped by the interplay of mass transport and local processes such as phase transitions and chemical reactions.[1] Familiar examples include dendrites[2], icicles[3], and speleothems[4], which feature characteristic shapes that are easily recognized but typically difficult to explain in quantitative terms. Other examples are generated by specific chemical reactions such as tubular precipitation structures in "silica garden" systems[5,6] and ultra-sharp tips produced for scanning tunneling microscopy (STM) by electrochemical etching[7].

The past decade has seen much progress towards mathematical models that are based on realistic physico-chemical processes and capable of describing the dynamics and shape selection in such systems. Perhaps the most important results of these efforts are the characterization of system-specific geometric attractors. Similar to the Platonic solids of ancient Greece some of these attractors are scale-independent, ideal forms. For instance, the intricate zinc metal leaves formed by quasi-two-dimensional electrodeposition are scale-invariant fractals and their Hausdorff dimension is reproduced by diffusion-limited-aggregation models.[8,9]

Stalactites are another example which—despite individual variations due to primarily external factors—obey a geometric growth law and a Platonic ideal. These cave structures result from the interplay of fluid flow, $CaCO_3$ chemistry, and CO_2 exchange between the thin solution layer covering the stalactite and the cave atmosphere. In 2005 Short *et al.* analyzed the stalactite shape in terms of the vertical height over its tip (z) and the corresponding radius (R) and obtained at large R the dependence $z \propto R^{4/3}$.[10,11] This power law was found to be in excellent agreement with the statistical average obtained from photos of natural stalactites. Despite major differences in the physical and chemical processes, ideal dripping icicles obey the same power law.[12,13]

The mathematical analysis of these two free-boundary problems leads to the same nonlinear ordinary differential equation for the asymptotic shape, but for icicles atmospheric heat transfer qualitatively takes the place of CO_2 exchange. In addition, both structures feature ripples around their circumference, which in the case of icicles result from dissolved ionic impurities.[14] In the case of stalactites, however, the ripples (crenulations) are closely linked to the hydrodynamics of the thin water film.[15] Lastly, we note that melting cylindrical blocks of ice in warm air also generate bullet-like forms that are reminiscent of the aforementioned examples.[13]

Here we report experimental data on a seemingly similar system: the dissolution of a macroscopic, amorphous object under the influence of gravity. The dissolution process clearly induces local density variations, which have the ability to trigger fluid convection. Such density-driven motion is of great fundamental and technological relevance capable of affecting a broad range of processes by enhancing reaction rates, sedimentation speeds, and heat transport[16,17]. One prominent example is the possible sequestration of CO_2 in deep saline formation for the mitigation of global warming, which also depends heavily on dissolution-induced convection.[18,19]

In the following, we will describe the dissolution of two model compounds in a large water reservoir. The shape of the dissolving object indeed approaches a geometric attractor but in contrast to

the scaling law for stalactites and icicles, we find a power law exponent of two. We suggest that in the presence of gravity, all amorphous objects undergoing dissolution approach this paraboloidal form.

EXPERIMENTAL METHODS

α-D-glucose (Sigma-Aldrich, anhydrous, 96 %) is carefully melted at 150 °C. Notice that higher temperatures induce unwanted caramelization.[20] The molten sugar is poured into a cylindrical Teflon mold (length 14 cm and inner diameter 2 cm) until it fills the entire bore volume (approximately 44 mL). A threaded rod with a handle is inserted as the sample cools to ambient temperature. After complete solidification, the glucose cylinder is removed from the mold. To minimize mechanical damage of the structure (such as thin cracks), the Teflon mold has a small hole at its base that allows for pressure equilibration. Furthermore, pre-lubrication of the bore with an oily liquid facilitates the sample extraction. After removal, the sample is mounted onto a holder in an upright position. The cylinder is then placed near the center of a rectangular reservoir (50 cm x 25 cm x 30 cm) filled with distilled water. The medium is covered to minimize fluid disturbances and other undesired effects. All dissolution experiments are conducted at room temperature. We also performed experiments with samples produced in smaller Teflon molds (length 10 cm and inner diameter 2 cm) that showed no qualitative differences in their dissolution dynamics but obviously resulted in shorter dissolution times.

A charge-coupled device camera (COHU 2122-1000) is used to collect image data of the dissolving object at 30 s intervals. In these experiments, the system is illuminated by diffuse, white light. The glucose cylinder dissolves completely within approximately 130 min. If the total amount of glucose were dissolved to produce a spatially homogeneous solution, it would have a concentration of approximately 8 mM, which is three orders of magnitude less than its solubility in water. We also studied the structure shortly before complete dissolution. The latter experiments employed an optical microscope (Leica DMIRB) and bright-field illumination.

Similar experiments are performed using polyethylene glycol (Sigma-Aldrich, average molar mass 4000 g/mol) which is melted at 65 °C. The total dissolution time in these experiments is about 320 min and therefore 2.5 times longer than the time needed to fully dissolve glucose samples of equal size and shape. In addition, PEG samples are more prone to cracking and subsequent dislodging of macroscopic fragments. To minimize this undesired effect, we varied the cooling rate during sample preparation but could not achieve noticeable improvements. Thinner structures show less cracking but also reduce the time to complete dissolution.

RESULTS AND DISCUSSION

Experimental Observations. Figure 1 illustrates the dissolution-driven evolution of an amorphous glucose (a) and polyethylene glycol (PEG) cylinder (b) in a tank holding 37 L of water. The solid cylinders are aligned vertically close to the center of the tank. In both cases the speed of the descending tip is much faster than the loss of material in radial direction at the base (see movies). Accordingly the samples acquire a bullet-like shape during the dissolution process. Notice that the initial structures are nearly perfect cylinders with a short conical cap (Figure 1c) and thin needle-like tip. The latter features correspond to the shape of the Teflon mold used for casting the samples. The fast dissolution of these small features creates initially a rather flat top (see second frames in Figures 1a,b) which then sharpens again to form the bullet-like shape. The structures shown in the third and fourth frames of Figures 1a,b have a similar shape suggesting the possible existence of a geometric attractor. During numerous experiments, we found that PEG samples are always more prone to cracking than otherwise identical glucose samples. For that reason PEG structures tend to lose millimeter-scale fragments, which impair subsequent analyses.

Several other features can be discerned from the image data in Figures 1, S1, and the corresponding movies (see Supporting Information). These features are related to local changes in the refractive index which must result from local concentration variations of the solute (i.e. glucose or PEG). Firstly, we observe a downward directed motion of faint, granular intensity variations close to the surface of the glucose cylinders. The intensity variations can be seen in the first frame of Figure 1a. Starting from the upper cylinder end, this weak signal diminishes within the first 30-50 min and yields a visually smooth surface. However, we often notice three to four dark, vertical stripes on the dissolving structure (see second frame of Figure 1a). Removal of the sample from the tank and swift visual inspection revealed no evidence for surface modulation that could correspond to these stripes. We hence attribute them to optical artifacts. Notice that for PEG samples we observe neither the initial granular pattern nor the later stripes. Secondly, we always detect an exhaust-like flow at the bottom of both glucose and PEG cylinders (Figures 1d,e). This downward directed flow starts during the first minutes of the experiment and continues until the object is fully dissolved. The horizontal width of the exhaust pattern decreases smoothly in the downward direction (Figures 1d,e). We interpret this pattern as a region of higher solute concentration within a thin layer of solution flowing down the sample surface. This flow clearly must initiate some fluid motion in the surrounding solvent that contains less or essentially no solute.

Quantitative Characterization. To characterize quantitatively the evolving shape, we extract the contour of the dissolving object from images at different time steps. A representative data set is shown in Figure 2 (red points). Notice that this figure over-emphasizes the width of the sample due to the different scaling of the ordinate and abscissa. For consistency, only the top 2.8 cm of the object are analyzed. This length yields a sufficiently large data set for fitting without shortening the analyzable time span significantly. During the late stages of the experiment, the tip shape was not fully retrieved by our method. In these cases, we obtain a discontinuous contour plot with some missing points. The contour

data are fitted with very good agreement to power laws of the form $z \propto R^k$ where z is defined as the vertical distance from the tip and R is the local radius (black, dashed line in Figure 2a). For the example shown, the power law exponent k is 2.06. We also calculate the residual values Δz between the experimental data and the fitted power law (Figure 2b). These values are small compared to the height of the sample and show no noteworthy trends. The root mean square values are typically less than 0.1 cm and generally decrease with time indicating better fits towards the end of the experiment.

Another approach for the analysis of power law data evaluates the logarithms of the dependent and independent variables, which should obey the linear equation $\log(z) = const + k \log(R)$. Compared to direct power law fits (see Figure 2), this method assigns more weight to the small z-value data at the tip of the sample. Its results are illustrated in Figure 3a for the example of six points in time during a representative glucose-dissolution experiment. The topmost data set (orange circles) represents the sample shape 122 min into the experiment, while the (magenta) star-shaped markers characterize a much earlier state (65 min). The data sets are analyzed individually by linear regression and the resulting graphs are superposed as continuous, black lines in Figure 3a. We find that the contours are well-described by the assumed power law, although the three earliest data sets show small deviations at large R values.

During the early stages of the experiments, the shape of the dissolving structure (and hence also k) is strongly affected by its arbitrary initial shape. Figures 3b,c quantify this process in terms of the power law exponents found by direct fitting and double-logarithmic fitting, respectively. In both cases, the data converge towards an exponent of about two. For the particular initial shape and size of our glucose samples, this transition requires approximately 100 min. The small difference in the decay time of these geometric transients between Figures 3b,c is attributed to a more rapid shaping of the top portion of the sample and the difference in the weighing of data points between the two methods. The analysis of several experiments at $t = 123$ min yields averages of $k_{pow} = 2.06 \pm 0.04$ for direct power law fits and $k_{log} = 1.99 \pm 0.02$ for log-log fits, which strongly suggests that the dissolving objects become paraboloids of revolution.

As additional evidence for the existence of the paraboloidal attractor and to directly address the question raised in the title of this Article, we create a master curve from the shape data of a representative glucose dissolution experiment. The analysis spans the time interval from 105 min to 120 min during which the sample's length shrinks by about one half. The contours are obtained at 30 s intervals and fitted to $z = AR^2$ to obtain the time-dependent scaling coefficients A (see Figure S3). Figure 4 shows our data in terms the dimensionless abscissa AR and the dimensionless ordinate Az. The rescaled contours are represented by different color markers and fall on a unique master curve. The superposed black curve graphs the expected function $Az = (AR)^2$ and is in excellent agreement with our measurements. Accordingly, we conclude that the dissolving glucose structure indeed converges to a universal shape.

The theoretical work on the ideal shape of stalactites and icicles notes that the simple geometric laws cease to hold close to the tip of the structures.[10-13] This limitation is primarily due to pendant drops detaching repeatedly from the structure's tip and therefore characterized by the capillary length which is about 0.3 cm for stalactites. In addition, a smaller—and hence irrelevant—cutoff is predicted by the

theory. Since the dissolution process does not involve pendant droplets but rather smooth fluid flow, we further investigate the shape of the dissolving structure close to the tip. Figure 5a shows an optical micrograph of a glucose sample in the final minutes before its complete dissolution. Because microscopy of the structure within the water tank is technically challenging, we remove the dissolving sample from the container and quickly dry it with compressed air to stop the dissolution. As for the larger image data, the contour of the micro-tip is in very good agreement with a parabola (Figure 5b). This finding shows that the paraboloidal shape persists down to a distance of at least a few tens of a micrometer from the tip.

Phenomenological Model. Lastly we discuss the dynamics of the structure once it has come sufficiently close to its geometric ideal. Figure 6a shows the temporal evolution of the sample radius R at three different heights z_0. These heights are constant within the reference frame of the laboratory. The end points ($R = 0$) of the individual data sets correspond to the time at which the tip passes through the corresponding height z_0. The error bars correspond to the length of one pixel in our image data. Notice that the rate dR/dt becomes more negative towards the end of the individual graphs. To account for the observed $R(t)$ dependence, we propose a simple, phenomenological model. It involves the dissolution rate $-v_0$ of a planar substrate surface and a curvature-dependent rate $-\delta/R$ that, in this simple model, is directly proportional to the curvature $1/R$:

$$\frac{dR}{dt} = -v_0 - \frac{\delta}{R} \qquad (1)$$

Notice that the last term in (2) creates faster dissolution for smaller objects. Integration yields the implicit, analytical solution

$$t - t_0 = \frac{R_0(z) - R(z)}{v_0} + \frac{\delta}{v_0^2} \ln \frac{R(z) + \delta/v_0}{R_0(z) + \delta/v_0} \qquad (2)$$

where the constant R_0 is the radius at some reference time (t_0 = 110 min for the data in Figure 6a).

Least-squares fits of Equation 2 are shown in Figure 6a and are in excellent agreement with the measurements. Each data set obtained at a particular z_0 value yields approximations of the model parameters v_0 and δ. Their resulting height-dependencies are shown in Figures 6b and c, respectively. In both cases, the parameters are essentially constant but show some weak and seemingly periodic variations caused by the pixel-based nature of the images. The data in Figures 6b and c have averages of $v_0 = (1.0 \pm 0.2) \times 10^{-2}$ cm/min and $\delta = (3.8 \pm 2.0) \times 10^{-4}$ cm^2/min. This result for the dissolution rate v_0 appears to have a plausible order of magnitude. Furthermore, the value for δ is rather close to the molecular diffusion coefficient of glucose at room temperature (4.0×10^{-4} cm^2/min)[21] but this similarity needs to be evaluated conservatively since transport in our system is strongly affected by convection. We also emphasize that Equation (1) cannot predict the convergence of an arbitrary shape towards a parabola and it does not preserve a parabola when it is used as the initial condition. It also yields less satisfactory results when compared to the downward motion of the tip (see Figure S2). Clearly a more

detailed analysis of the convection-diffusion-dissolution dynamics is needed, perhaps along the lines of recent work on icicle melting.[13]

CONCLUSIONS

In summary, we have shown that in a large container the dissolution of glucose and PEG cylinders results in paraboloidal shapes. Based on our experiments, we propose that all amorphous, soluble samples approach this geometric attractor. Consequently, the paraboloid is the Platonic ideal for dissolution in the presence in gravity. The power law exponent ($k = 2$) differs from the exponent ($k = 4/3$) reported for dripping stalactites and icicles which describe more pointed shapes. Moreover, one can expect that dissolving objects converge to spherical shapes in the absence of gravity and density-driven convection.

We suggest the following mechanism: during the early stage of dissolution, the solute concentration increases around the sample surface. This increase induces density changes that cause an unstable layering of heavy (solute-rich) solution over the lighter solvent and hence a downward directed flow along the sample surface. Notice that this motion is evident from the "exhaust-like" pattern at the base of the sample. Due to volume conservation in the incompressible fluid, this flow must be accompanied by an upward directed fluid movement further away from the sample and it seems likely that the dissolution process drives a large-scale convection roll centered along the structure's long axis. Moreover, we propose that the steady convection down the surface causes a smooth concentration gradient with very low solute concentrations around the top end of the structure and higher concentrations at the base. Accordingly, dissolution rates decrease from top to bottom and therefore qualitatively explain the rapid loss of material in the tip region and the much slower loss at the base. We reemphasize that these rates are solute-dependent as exemplified by the two examples studied here.

This convection-dissolution mechanism is affected by solute diffusion that defines the thickness of the solute layer around the dissolving structure. This thickness increases from zero at the tip to positive values at the base according to the solute diffusion coefficient and the velocity profile of surrounding fluid. We estimate that the transit time of the fluid down the structure is of the order of minutes and hence should confine the solute to a rather thin (possibly sub-millimeter) envelope around the structure. Future experiments should aim to characterize this feature quantitatively and could be based on measurements of the solution's refractive index or optical rotation. Other experiments are needed to analyze the flow velocities in the system. However, such measurements are complicated by local density variations.

ASSOCIATED CONTENT

Supporting Information

Magnified views of the granular intensity variations and dark stripes observed on early glucose samples. Additional figures quantifying the temporal evolution of the sample radius at a certain height and the vertical descent of the sample tip. This material is available free of charge via the Internet at http://pubs.acs.org.

Web Enhanced Objects

Two time-lapse movies of a dissolving glucose and PEG sample.

AUTHOR INFORMATION

* E-mail: steinbck@chem.fsu.edu

Notes: The authors declare no competing financial interest.

ACKNOWLEDGMENTS

This work was supported by the National Science Foundation under Grants No. 1005861 and 1213259. We thank Jakob Löber (TU Berlin) for discussions.

REFERENCES

(1) Ball, P. *The Self-Made Tapestry: Pattern Formation in Nature;* Oxford University Press: New York, 2001.

(2) Meng, X. K.; Tang, S. C.; Vongehr, S. A Review on Diverse Silver Nanostructures. *J. Mater. Sci. Technol.* **2010**, *26*, 487-522.

(3) Makkonen, L. A Model of Icicle Growth. *J. Glaciol.* **1988**, *34*, 64-70.

(4) Hill, C. A.; Forti P. *Cave Minerals of the World,* 2nd Ed.; National Speleological Society: Huntsville, Alabama, 1997.

(5) Cartwright, J. H. E.; García-Ruiz, J. M.; Novella, M. L.; Otálora, F. Formation of Chemical Gardens. *J. Colloid Interface Sci.* **2002,** *256*, 351-359.

(6) Thouvenel-Romans, S.; Steinbock, O. Oscillatory Growth of Silica Tubes in Chemical Gardens. *J. Am. Chem. Soc.* **2003,** *125,* 4338-4341.

(7) Fotino, M. Tip Sharpening by Normal and Reverse Electrochemical Etching. *Rev. Sci. Instrum.* **1993**, *64*, 159-167.

(8) Matsushita, M.; Sano, M.; Hayakawa, Y.; Honjo, H.; Sawada, Y. Fractal Structures of Zinc Metal Leaves Grown by Electrodeposition. *Phys. Rev. Lett.* **1984,** *53*, 286-289.

(9) Witten, T. A.; Sander, L. M. Diffusion-limited Aggregation, a Kinetic Critical Phenomenon. *Phys. Rev. Lett.* **1981,** *47*, 1400-1403.

(10) Short, M. B.; Baygents, J. C.; Beck, J. W.; Stone, D. A.; Toomey III., R. S.; Goldstein, R. E. Stalactite Growth as a Free-Boundary Problem: A Geometric Law and Its Platonic Ideal. *Phys. Rev. Lett.* **2005,** *94*, 018501.

(11) Short, M. B.; Baygents, J. C.; Goldstein, R. E. Stalactite Growth as a Free-boundary Problem. *Phys. Fluids* **2005,** *17*, 083101.

(12) Short, M. B.; Baygents, J. C.; Goldstein, R. E. A Free-boundary Theory for the Shape of the Ideal Dripping Icicle. *Phys. Fluids* **2006,** *18*, 083101.

(13) Neufeld, J. A.; Goldstein, R. E.; Worster, M. G. On the Mechanisms of Icicle Evolution. *J. Fluid Mech.* **2010,** *647*, 287-308.

(14) Chen, A. S. H.; Morris, S. W. On the Origin and Evolution of Icicle Ripples. *New J. Phys.* **2013,** *15*, 103012.

(15) Camporeale, C.; Ridolfi, L. Hydrodynamic-Driven Stability Analysis of Morphological Patterns on Stalactites and Implications for Cave Paleoflow Reconstructions. *Phys. Rev. Lett.* **2012,** *108*, 238501.

(16) Ahlers, G.; Grossmann, S.; Lohse, D. Heat Transfer and Large Scale Dynamics in Turbulent Rayleigh-Bénard Convection. *Rev. Mod. Phys.* **2009,** *81*, 503-537.

(17) Alamarcha, C.; Trevelyan, P. M. J.; Grosfils, P.; De Wit, A. Chemically Driven Hydrodynamic Instabilities. *Phys. Rev. Lett.* **2010,** *104*, 044501.

(18) Hassanzadeh, H.; Pooladi-Darvish, M.; Keith, D. W. Scaling Behavior of Convective Mixing, with Application to Geological Storage of CO_2. *AIChE J.* **2007,** *53*, 1121-1131.

(19) Tsai, P. A.; Riesing, K.; Stone, H. A. Density-driven Convection Enhanced by an Inclined Boundary: Implications for Geological CO_2 Storage. *Phys. Rev. E.* **2013,** *87*, 011003.

(20) Hodge, J. E. Dehydrated Foods, Chemistry of Browning Reactions in Model Systems. *J. Agric. Food Chem.* **1953**, *1*, 928-943.
(21) *Handbook of Chemistry and Physics* (76th ed.); Lide, D. R., Ed.; CRC Press: Boca Raton, 1995.

FIGURE CAPTIONS

Figure 1. Shape evolution of a soluble cylinder in a large water tank. (a) Glucose cylinder 5, 50, 90, and 110 min after the start of dissolution experiment. The red, dotted lines are spaced at 2.8 cm (the length interval used in subsequent analysis). (b) Polyethylene glycol cylinder at 5, 150, 200, and 250 min. Individual image size: 14 cm x 4 cm. (c) Photo of the initial sample shape. The sample has a diameter of 2 cm and a funnel-shaped cap. (d,e) Photos of patterns related to the solution's refractive index at the base of a dissolving glucose and PEG sample, respectively. Image size: 1.95 cm x 2.05 cm.

Figure 2. Analysis of the top 2.8 cm of a glucose sample after 115 min of dissolution. (a) Contour of the structure (red points) and fitted power law (black, dashed line). The corresponding power law exponent is $k_{pow} = 2.06$. (b) Residual values in z-direction between the experimental data and the fit. The dashed line corresponds to the root-mean-square value of 0.056 cm.

Figure 3. (a) Double logarithmic plots of the contour of a representative glucose sample at six different times t after the start of a dissolution experiment. The power law exponent k_{log}, measured as the slope of the linear fits (black, continuous lines), decreases monotonically. The k_{log} and t values are, respectively: 3.16, 65 min (magenta stars), 2.53, 70 min (grey triangles), 2.29, 77.5 min (green crosses), 2.23, 92.5 min (red dots), 2.12, 107.5 min (blue plus signs), and 2.09, 122.5 min (orange circles). (b,c) Temporal evolution of the power law exponent as obtained from several experiments. The data in (b) and (c) are results from direct power law fits and linear regression of double logarithmic data, respectively.

Figure 4. Master curve of thirty rescaled contours of a dissolving glucose structure in terms of the dimensionless variables Az and AR where A is the time-dependent steepness of the parabolic sample contour. Different color markers denote different times during the 15 min interval towards the end of the dissolution process. The continuous, black curve is the graph of $Az = (AR)^2$.

Figure 5. (a) Optical micrograph of the upper portion of the glucose structure after 125 min of dissolution. Scale bar: 50 μm. (b) Contour of the micro-tip (red dots) and the least squares fitted parabola (black dashed line).

Figure 6. Analysis of glucose dissolution. (a) Sample radius R as a function of time for three heights z_0 in the reference frame of the laboratory. The continuous lines are least squares fits using Eq. (2), which each yield a transport coefficient δ and a dissolution speed v_0. The latter parameters are plotted in (b,c) for a range of z_0 values. The colored markers correspond to the examples in (a). The continuous lines represent the average values of δ and v_0.

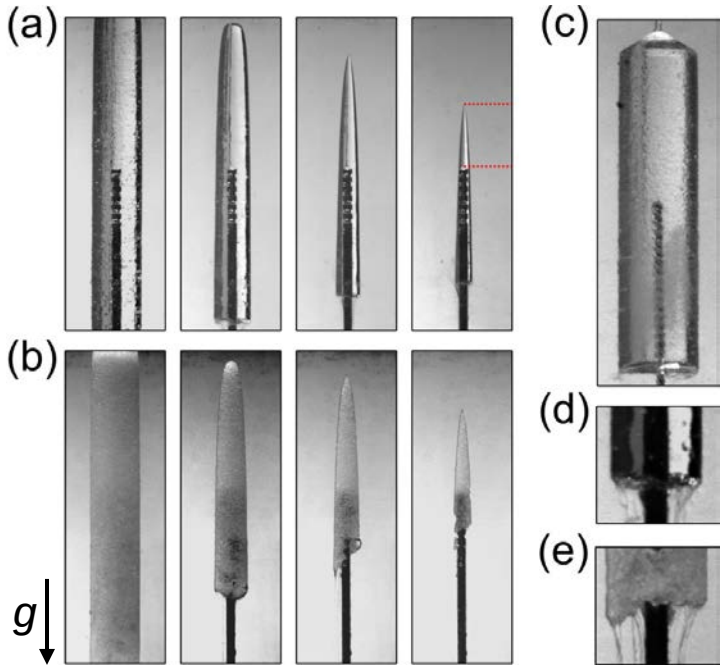

Figure 1

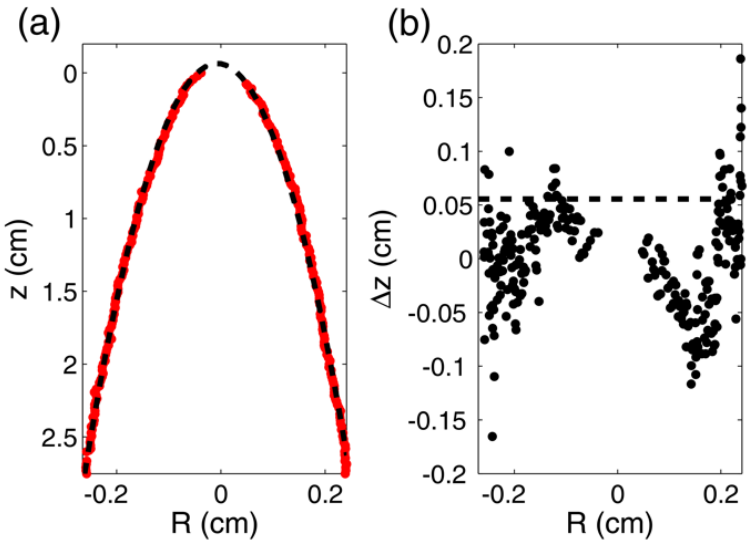
(a)
(b)
z (cm)
R (cm)
Δz (cm)
R (cm)
0
0.5
1
1.5
2
2.5
-0.2
0
0.2
0.2
0.15
0.1
0.05
0
-0.05
-0.1
-0.15
-0.2

Figure 2

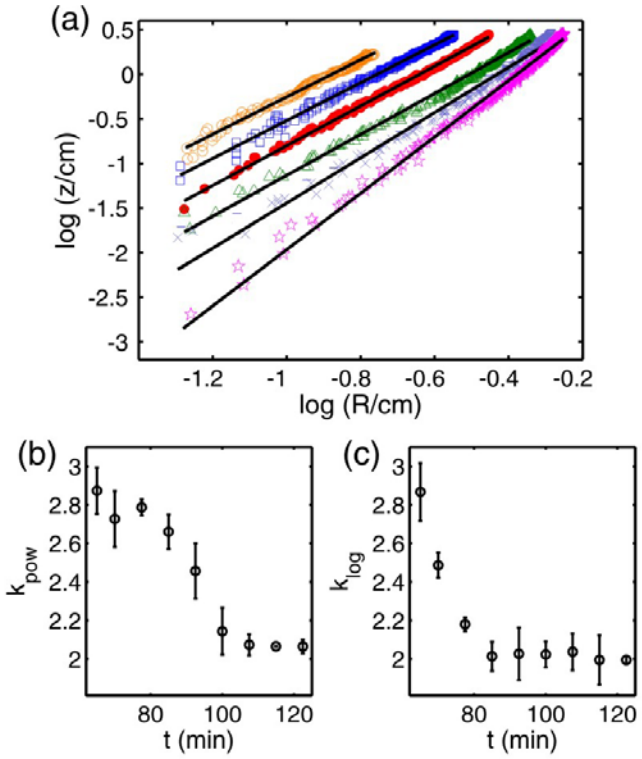
(a)
log (z/cm)
log (R/cm)
0.5
0
-0.5
-1
-1.5
-2
-2.5
-3
-1.2
-1
-0.8
-0.6
-0.4
-0.2
(b)
k_{pow}
t (min)
(c)
k_{log}
t (min)
3
2.8
2.6
2.4
2.2
2
80
100
120

Figure 3

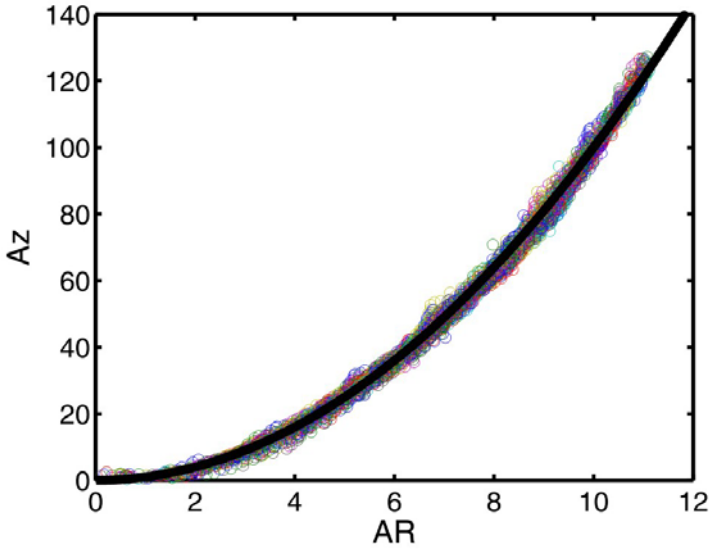

Figure 4

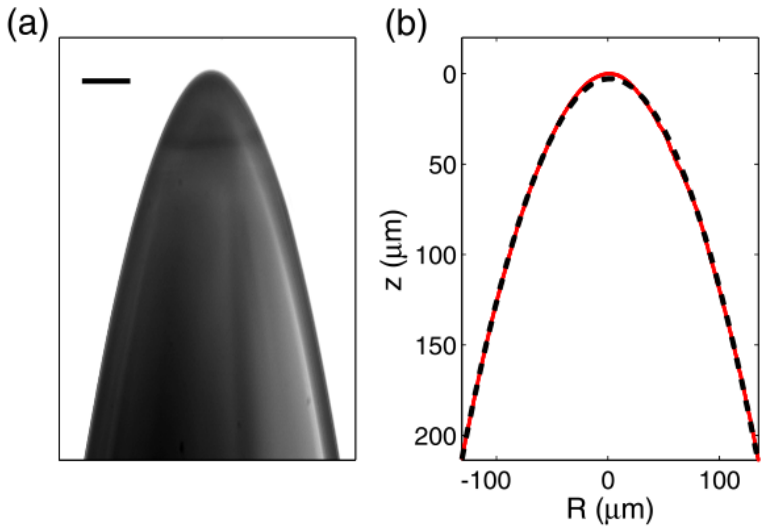

Figure 5

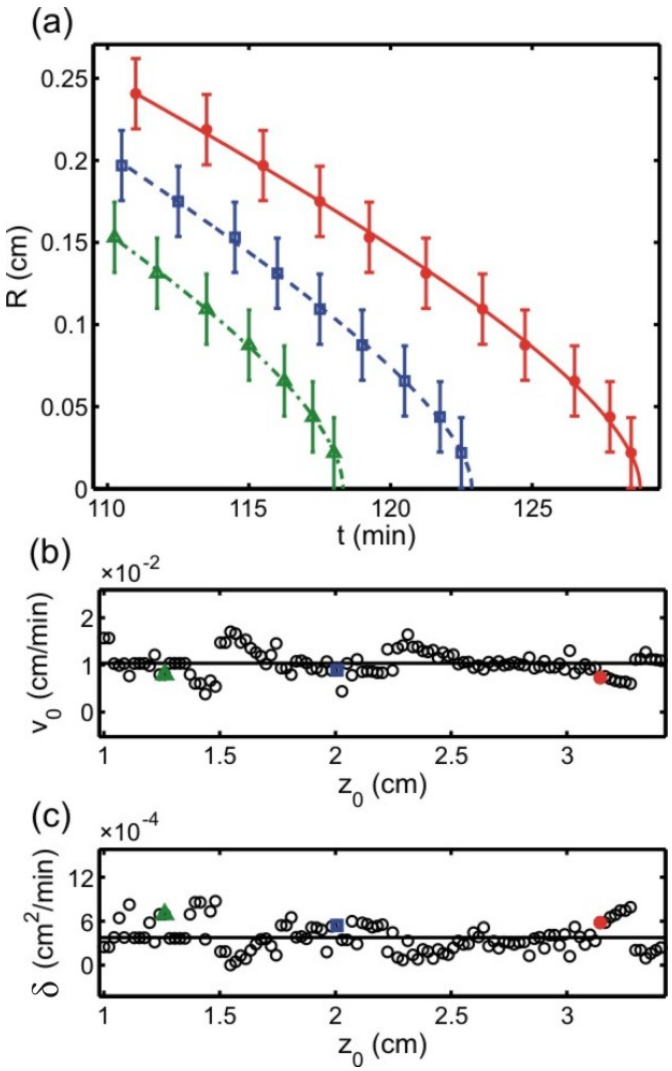
(a)
R (cm)
0.25
0.2
0.15
0.1
0.05
0
110
115
120
125
t (min)
(b)
×10^-2
v0 (cm/min)
2
1
0
1
1.5
2
2.5
3
z0 (cm)
(c)
×10^-4
δ (cm^2/min)
12
6
0
1
1.5
2
2.5
3
z0 (cm)

Figure 6

TOC Graphic